analytical chemistry

pubs.acs.org/ac Article

Flexible Microfluidic Devices for Tunable Formation of Double Emulsion

Uditha Roshan, Ajeet Singh Yadav, Xiaoyue Kang, Du Tuan Tran, Amith Mudugamuwa, Jun Zhang,* and Nam-Trung Nguyen*

Cite This: https://doi.org/10.1021/acs.analchem.5c00338 Read Online

ACCESS | Metrics & More | Article Recommendations | Supporting Information

ABSTRACT: Double emulsions are highly structured dispersion systems that generate double-layered droplets. Double emulsions offer an effective platform for encapsulating liquid samples. Multilayer protection, controlled release of encapsulated materials, and stability make double emulsions superior to single emulsions in handling sensitive liquid samples. This technology is widely used in biology, food technology, cosmetics, and environmental sciences. Microfluidic emulsification is a promising method for producing highly monodisperse double-emulsion droplets with a high encapsulation efficiency. Well-controlled adjustment of the core size and shell thickness is critical for applications of double emulsions. Changing the flow rates of the fluid phases is the most straightforward method to control the emulsion sizes. However, monodisperse double-emulsions can only be generated within a small range of flow rates. Thus, producing monodisperse double emulsions with a wide size range without changing the device design or drastically altering the fluid properties is challenging. Here, we demonstrate a facile method to generate monodisperse double-emulsion droplets with tunable core size and shell thickness without changing the flow rates of the fluid phases. To address this challenge, we developed a proof-of-concept flexible and stretchable microfluidic device capable of controlling core size, shell thickness, and generation frequency by adjusting channel dimensions and stretching the microfluidic device. We incorporated three stretching cases to assess the feasibility of controlling the generation process of the double emulsion. We demonstrated that stretching increases the core size and shell thickness and decreases the generation frequency. Experimental results showed an ∼84% increase in core volume and an ∼23% increase in shell volume by applying ∼16% device strain. This innovative approach significantly advances the field of droplet-based microfluidics, providing on-site, real-time tunability for the generation of double-emulsion droplets with high precision and reproducibility.

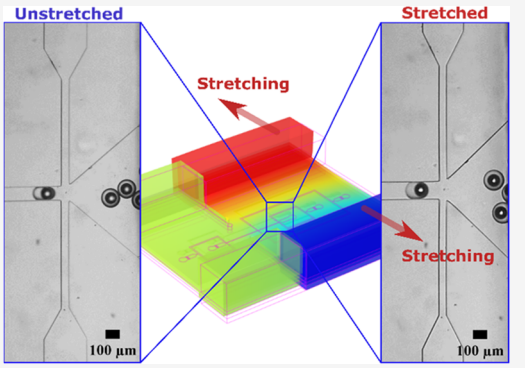

Downloaded via Nam-Trung Nguyen on March 7, 2025 at 03:19:50 (UTC).
See https://pubs.acs.org/sharingguidelines for options on how to legitimately share published articles.

INTRODUCTION

Double emulsions are complex fluid systems with three immiscible liquid phases separated by at least two interfaces.[1] A double-emulsion droplet consists of an inner fluid core encapsulated by a middle fluid layer that is further dispersed in an outer fluid. In general, these distinct fluid domains are defined as the core, shell, and carrier fluid phases. This core−shell structure enables the encapsulation of liquid samples in a container,[2] which is more stable than single emulsions and capable of systematically controlling the encapsulated phase. Due to this unique advantage, double-emulsion droplets have received significant attention in applications such as cell analysis,[3] drug delivery,[4] food and beverage,[5] cosmetics and personal care industries,[6] as well as environmental remediation.[7,8] In addition, core−shell particles synthesized through double-emulsion droplets are considered more stable carriers than single-emulsion droplets. These core−shell microcapsules can be used to make stable assays for precise molecule quantification using techniques such as digital loop-mediated isothermal amplification (dLAMP).[9]

Double-emulsion droplets can be formed through various methods.[10−12] Bulk methods, including two-step agitation, high-shear mixing, and sonication, typically produce highly polydisperse droplets with limited size control. These methods are suitable for large-scale production, where monodispersity is less critical. In contrast, microfluidic emulsification has emerged as a promising method due to its versatility and robustness. Microfluidics can produce highly monodisperse droplets with excellent encapsulation efficiency.[10,13,14] Similar to the microfluidic generation of a single emulsion, capillary instability under inertial and viscous forces facilitates double-emulsion formation. Hence, the characteristics of double-emulsion droplets depend on parameters such as the properties

Received: January 15, 2025
Revised: February 21, 2025
Accepted: February 28, 2025

© XXXX American Chemical Society

https://doi.org/10.1021/acs.analchem.5c00338
Anal. Chem. XXXX, XXX, XXX−XXX

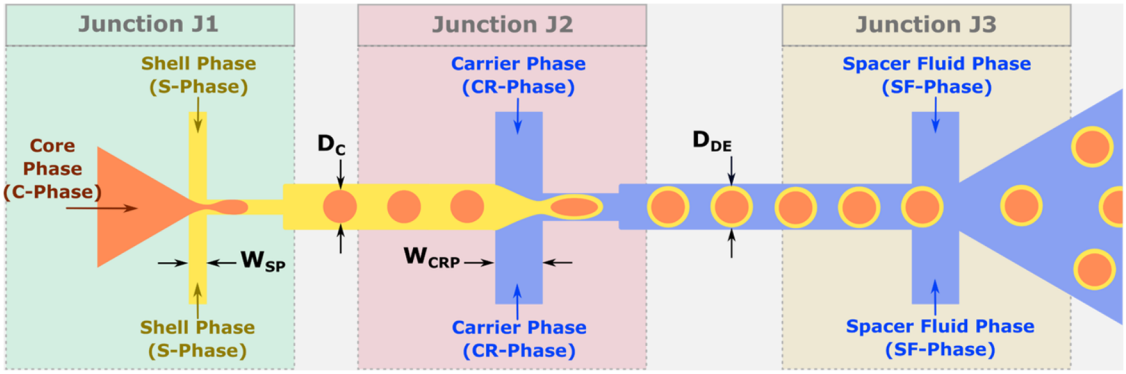

Figure 1. Parameters considered for theoretical analysis and the fluid phases involved in the generation of double emulsion.

of the three phases,[15] flow rates of individual phases, surface wettability, and microchannel geometry.[14] Among these parameters, microchannel geometry has been found to have the most significant impact on the double-emulsion characteristics. Galogahi et al.[16] reported that doubling the channel width increased the radius of the generated core droplets and core−shell droplets by 50−60% and 60−70%, respectively. However, the change in flow rates did not significantly vary the sizes. This is primarily because droplet pinch-off dynamics, which largely determine core and shell volumes, are more sensitive to changes in channel dimensions than flow rates.[17]

The size tunability of the double emulsion is essential in many applications. For instance, lipid oxidation significantly affects the quality of food emulsions.[18] Reducing the size of the core droplet increases the surface area, increasing the concentration of reactants at the droplet surface, which in turn increases the lipid oxidation rates. Thus, tuning the droplet size can control the lipid oxidation rate and minimize the quality deterioration of food emulsions. In addition, the relative sizes of the inner and outer phases also affect the stability and release mechanisms of double emulsions loaded with bioactive compounds.[19] Reducing the ratio of the inner-to-outer droplet size can decrease the release rate of bioactive compounds. Tuning the size of the double-emulsion droplets can also enhance encapsulation efficiency and stability. Beyond controlling the encapsulated active components, the characteristics of double emulsions also significantly affect their manipulation capabilities. In a recent study,[20] we reported the synthesis of magnetic liquid beads suitable for active manipulation. These beads featured a polymer shell containing magnetic particles. By precisely controlling the shell volume during the formation process, we created liquid beads with varying amounts of magnetic particles in the shell, resulting in tunable magnetization. To date, the formation of a double emulsion primarily relied on adjusting the flow rates of core, shell, and carrier phases. However, the flow parameters can only be changed within a narrow margin for a particular device geometry to obtain monodisperse double emulsions.[21] The core generation frequency at the first flow-focusing junction must be matched to the second emulsion generation frequency at the second junction. Because of the frequency mismatch, the double emulsion has a high polydispersity outside this range of flow rate. Given that microchannel dimensions significantly affect the characteristics of double emulsions,[16] it will be more promising to control the formation process in real time with tunable channel dimensions.

In this work, we developed a fully flexible and stretchable microfluidic technology for tunable formation of double emulsion and core−shell liquid beads. The channel dimensions of the proposed flexible device can be precisely adjusted through external stretching,[22] enabling control over parameters such as core volume, shell volume, and generation frequency. We selected the two-step flow-focusing configuration and conducted a theoretical analysis to elucidate the effect of stretching on double-emulsion formation. Next, we fabricated a flexible and stretchable microfluidic device that independently facilitates the stretching of the individual flow-focusing junctions of the two corresponding stages. The core size can be tuned by stretching the first junction, and the shell thickness can be adjusted by stretching the second junction. We then experimentally evaluated the double-emulsion characteristics under three cases: stretching junction 1, stretching junction 2, and stretching the entire device.

THEORETICAL ANALYSIS

Our previous work[23] comprehensively investigated the effect of channel dimension on droplet formation. Since the present work uses the same flow-focusing configuration to generate the core droplet in the first stage and double-emulsion droplet in the second stage, the size of the core and double emulsion can be predicted by the power law as follows. The normalized sizes of the core $\left(\frac{D_C}{w_{SP}}\right)$ and double emulsion $\left(\frac{D_{DE}}{w_{CRP}}\right)$ can be predicted by[23]

$$\frac{D_C}{w_{SP}} = \frac{D_{DE}}{w_{CRP}} = k_{ij}\alpha_j^{m_{ij}} \quad (1)$$

where D_C and w_{SP} are the core diameter and the channel width of the shell phase, respectively, Figure 1. D_{DE} and w_{CRP} are the outer diameter of the double emulsion and the channel width of the carrier phase, respectively. α_j is the stretching variable, and k_{ij} and m_{ij} are the scaling law coefficients for the core/double-emulsion size. The subscript j = 1 and 2 denotes the corresponding junction, and the subscript i = 1, 2, and 3 denotes the stretching case. For example, k_{11} and m_{11} denote the scaling law coefficients for core generation under junction 1 stretching. k_{32} and m_{32} denote the scaling law coefficients for double-emulsion generation at junction 2 under stretching the entire device. Following are all the states of these variables,

https://doi.org/10.1021/acs.analchem.5c00338
Anal. Chem. XXXX, XXX, XXX−XXX

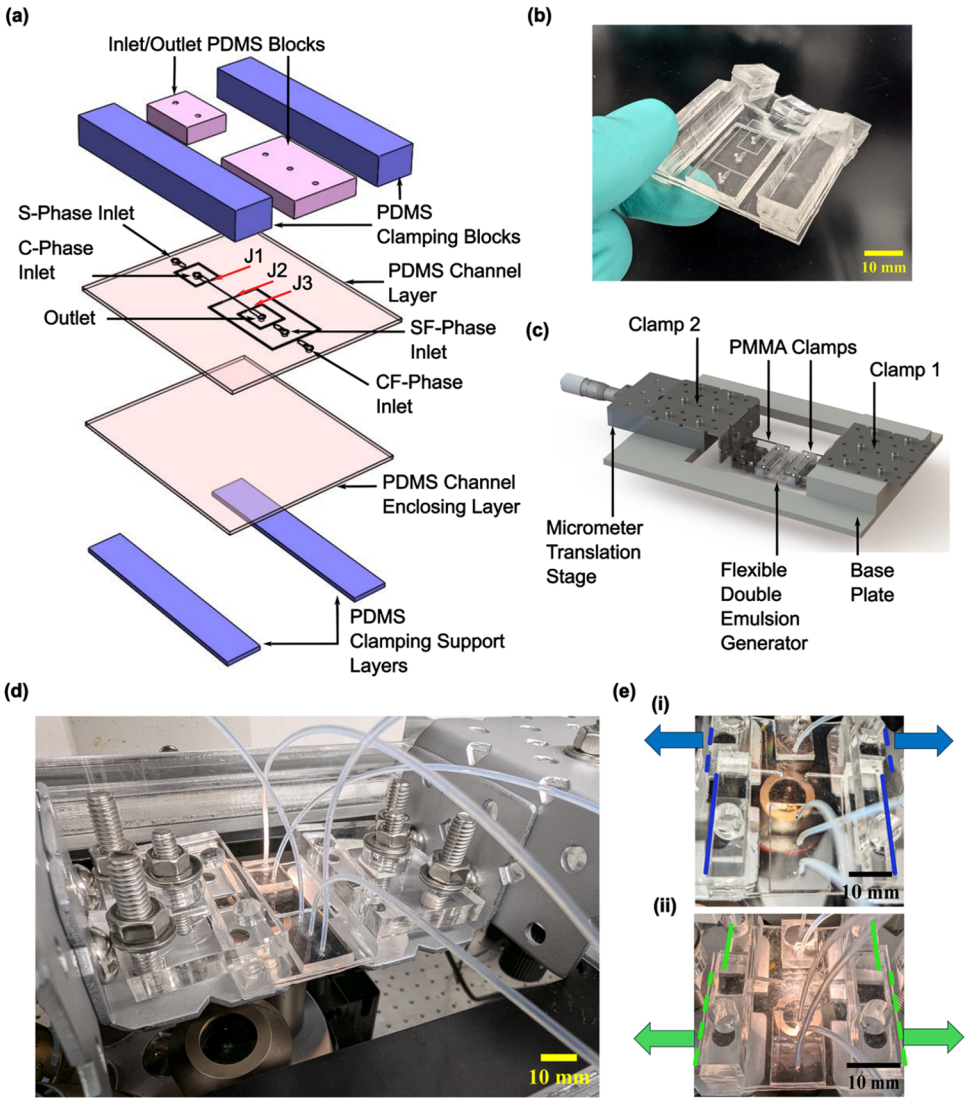

Figure 2. (a) Schematic configuration of the stretchable double-emulsion generator. (b) A photograph of the flexible PDMS microfluidic device. (c) Schematic assembly of the flexible microfluidic double-emulsion generator and the stretching platform. (d) A photograph of the experimental setup. (e) Flexible double-emulsion generator at different stretching modes: (i) Stretching of junction 1; (ii) Stretching of junction 2.

$$\begin{bmatrix} k_{11} & k_{12} \\ k_{21} & k_{22} \\ k_{31} & k_{32} \end{bmatrix}, \begin{bmatrix} m_{11} & m_{12} \\ m_{21} & m_{22} \\ m_{31} & m_{32} \end{bmatrix}, [\alpha_1 \quad \alpha_2]$$

In addition, core and double-emulsion pinch-off time (t_p'') can be predicted as

$$t_p = k'_{ij}\alpha_j^{m'_{ij}} \tag{2}$$

where k'_{ij} and m'_{ij} are the scaling law coefficients for pinch-off time related to core and double-emulsion droplets. Stretching variables for cores (α_1) and double-emulsion droplets (α_2) are described as

$$\alpha_1 = 1 + \frac{\Delta w_{SP}}{w_{SP}} \tag{3}$$

$$\alpha_2 = 1 + \frac{\Delta w_{CRP}}{w_{CRP}} \tag{4}$$

Equations 1 and 2 indicate that the core-double-emulsion size and generation frequency are sensitive to the strain applied to the device. If the values of m and m' are positive, stretching along the lateral direction will increase the size of core/double-emulsion and decrease the generation frequency. In contrast, if the values of m and m' are negative, stretching the device along the lateral direction will reduce the size of the core/double-emulsion and raise the generation frequency. We can also estimate the value of m and k (or m', k') by fitting experimental data with an exponential function. In addition, Supporting Information S-1 provides a more fundamental description of double-emulsion formation under device elongation.

MATERIALS AND METHODS

Device Design and Fabrication. The two-step flow-focusing devices used in our experiments have four inlets for core (C-Phase), shell (S-Phase), carrier (CR-Phase), and spacer (SF-Phase) phases as well as an outlet (Figure 2a). The symmetric S-Phase channels meet the C-Phase orifice at 90° at the first flow-focusing junction J1. The symmetric CR-Phase

https://doi.org/10.1021/acs.analchem.5c00338
Anal. Chem. XXXX, XXX, XXX−XXX

meets the core droplet output channel at 90° at the second flow-focusing junction J2. Both flow-focusing junctions were designed with constrictions to enhance droplet pinching. The initial widths of the S-Phase channel and C-Phase orifice are 50 μm. The constriction has a width of 30 μm and a length of 450 μm. The constriction facilitates hydrodynamic focusing of the two fluids and forms the core droplet in S-phase fluid. Downstream to the first constriction is the 100-μm core outlet channel leading to the second flow-focusing junction J2. We considered three designs for fabricating rigid microfluidic devices for the initial experiments. The corresponding width of the second constriction was set to 50, 60, and 70 μm. In addition, we selected the device with 50 μm constriction width at the second junction to fabricate flexible devices. In all designs, the second constriction is 450 μm long. Downstream to the second constriction is the outlet of the double emulsion. The 100-μm outlet channel meets the symmetric SF-Phase channels at the third junction J3. After the third junction, the double-emulsion droplets flow through a 1 mm channel toward the outlet port. All channel sections have the same height of ~130 μm.

The microfluidic devices were fabricated using standard photolithography and soft lithography techniques.[24] SU-8 3050 negative photoresist from MicroChem Corp. was used to develop the mold on a silicon wafer. Poly(dimethylsiloxane) (PDMS) (SYLGARD 184, Dow Corning, MI) prepolymer was thoroughly mixed with curing agent at a 10:1 ratio and subsequently degassed and poured onto the SU-8 mold. In making flexible microfluidic devices, the amount of polymer mixture was adjusted to achieve an ~750-μm thin PDMS channel layer. The mold was then kept in a properly leveled oven at 75 °C for ~2 h to allow PDMS to solidify evenly throughout the mold. Next, the solidified PDMS channel layer was carefully peeled off. Subsequently, an ~750-μm thin PDMS cover layer was bonded to the channel layer. Two ~3 mm thick PDMS blocks were bonded on top of the channel layer to facilitate the inlet and outlet tubing connection. Finally, two PDMS clamping supporting slabs (~6 mm) and two PDMS clamping supporting layers (~1 mm) were bonded along both sides of microchannels on top and bottom of the thin PDMS layers (Figure 2a), respectively. All PDMS-to-PDMS bonding processes were performed with an oxygen plasma treatment. The fabrication process was described in detail in our previous works.[23,25]

Surface modification of the microchannels is required to successfully form double-emulsion droplets. Sections of the microchannels were treated with poly(vinyl) alcohol (PVA) to make it hydrophilic.[26] A 1% w/v PVA solution was prepared by mixing with deionized (DI) water using a magnetic stirrer at 90 °C for 30 min. Following the bonding process, the microchannels were immediately flooded with a PVA (87−90% hydrolyzed, average mol wt. 30,000−70,000, Sigma-Aldrich) solution and kept on a hot plate at 120 °C for 7 min. The channels were then dried with nitrogen gas. This process was conducted three times to ensure a sufficient level of hydrophilicity. Finally, the flexible microfluidic device was partially dissected along the lateral direction to selectively perform stretching experiments on individual flow-focusing junctions, Figure 2b.

Discrete and Continuous Fluid Phases. Using the devices described above, droplets of fluorinated oil (HFE, Novec 7500 3M) were generated at the first flow-focusing junction using trimethylolpropane trimethacrylate (TMPTMA, Sigma-Aldrich Co.) as the S-Phase. Here, HFE 7500 and TMPTMA droplets were chosen to generate HFE 7500 monodispersed droplets.[21,27] In addition, TMPTMA has good chemical compatibility and high thermal stability[28] when it comes to applications such as digital polymerase chain reaction.[21] An aqueous solution of 50% glycerol (Chemsupply) with 0.06 mM Tween 20 was used as the CR-Phase for the second junction J2 to encapsulate the core droplet. In addition, the same fluid was used as the SF-Phase at third junction J3. Table S1 lists the fluid properties at 25 °C.

Experimental Setup. The experimental setup for the flexible microfluidic device consists of a stretching platform,[25] Figure 2c, an optical microscope with a high-speed camera, and four syringe pumps. The stretching platform consists of a micrometer translation stage on a PMMA base. Two metal clamps were attached to the base plate and the micrometer translation stage. Two PMMA slabs positioned the flexible PDMS device between the metal clamps. After clamping, the translational stage was adjusted to make the flexible device recover its initial deformations before experiments. The initial channel lengths were measured as a reference while the translation stage was adjusted to ensure that the device was precisely stretched.

The stretching platform with the PDMS device was placed on the stage of an inverted microscope (ECLIPSE Ti2, Nikon, Japan), Figure 2d. Four syringe pumps (NEM-B101-03A, CETONI GmbH, Germany) controlled the flow rates of the core, shell, carrier, and spacer phases. A high-speed camera (Chronos 2.1-HD High-Speed Camera, Kron Technologies Inc., Canada) was mounted on the microscope, and videos were recorded with an exposure time of 30 μs. The camera captured the formation processes at the flow-focusing junctions J1 and J2, as well as the formed double-emulsion droplets at the outlet. The recorded videos were analyzed using open-source software ImageJ (National Institutes of Health). Quantitative data of the core, shell, and double-emulsion droplets were then extracted. In addition, the core diameters were analyzed using Droplet Morphometry and Velocimetry (DMV) software.[29]

Experimental Procedure. First, we fabricated PDMS−PDMS rigid devices of the three designs mentioned above to identify the optimum flow rates of the three phases and the geometrical parameters to produce a monodisperse double-emulsion. More details of this work can be found in Supporting Information S-4. After identifying these parameters, we fabricated PDMS−PDMS flexible devices following the fabrication procedure mentioned in the previous subsection. Next, we investigated the effect of stretching on the characteristics of double-emulsion droplets, such as the size of the core and the double-emulsion droplets as well as their formation frequencies.

For the flexible devices, experiments were conducted at various elongations (0−4 mm) by adjusting the translation stage. This corresponds to a maximum device strain of 16% which is in the elastic region of the PDMS material. We opted not to go beyond this strain to ensure that the device provides consistent dimensional changes when undergoing stretching and stretch-releasing cycles, which, in turn, give consistent results. On the other hand, higher strains could cause delamination of PDMS layers, causing fluid leakages and device failures. We used the same flow rate conditions found in the initial experiments with rigid devices. Following tests were conducted to evaluate the effect of stretching on the core size,

https://doi.org/10.1021/acs.analchem.5c00338
Anal. Chem. XXXX, XXX, XXX−XXX

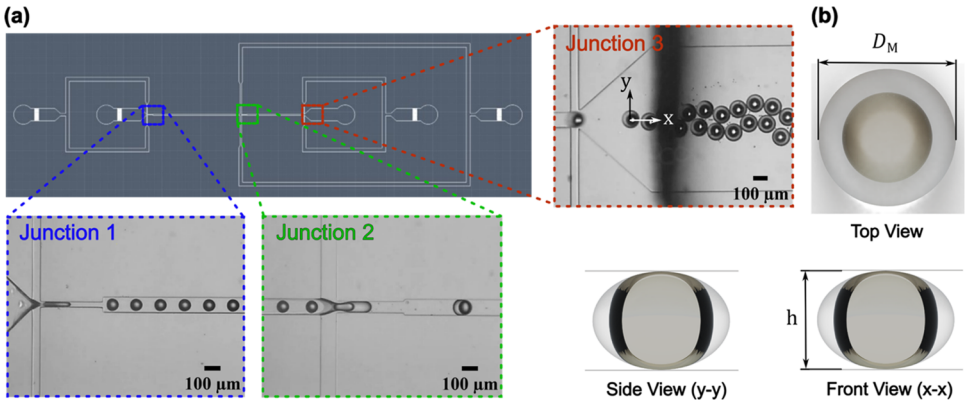

Figure 3. Formation of double-emulsion droplets in a two-step flow-focusing microfluidic device. (a) The core droplets are formed at junction 1 by pinching-off core fluid by the shell fluid stream. The formed core droplets are then encapsulated at junction 2 in shell fluid by pinching-off shell fluid by the carrier fluid stream. Finally, the spacer fluid stream directs the formed double-emulsion droplets toward the outlet. (b) Schematic illustration of double-emulsion droplet confined by the channel walls ($h < D_M$) and obtaining an ellipsoidal shape.

shell thickness, as well as formation frequencies: (i) Stretching only the first flow-focusing junction, Figure 2e(i); (ii) stretching only the second flow-focusing junction, Figure 2e(ii); (iii) stretching the entire device. In these tests, the flow rate (Q_{SF}) of the spacer fluid was kept constant at 800 μL/h.

The device was stretched with 1 mm step. Once the formation process stabilized, videos of each junction were captured (Figure 3a) (Video S1). Videos were recorded 1 min after stretching or adjusting the flow rate to a new setting. Each video of junction J1 has on average 600 frames. A frame contains 10−15 droplets depending on the elongation. The diameter and the generation frequency of the core droplets before encapsulation were determined. Each video of junction J2 has 1500 frames on average. About 50 consecutive double-emulsion droplets were captured after junction J3. The mean and standard deviation of the population were calculated for each stretching case. In addition, normal distribution curves for the population were used to identify the size distribution of the double-emulsion droplets. The double-emulsion characteristics are presented as box plots and normal distribution curves for a particular elongation. Features of the box plot indicate the 25 and 75% quartiles, median, minimum, and maximum values of the data. Double-emulsion droplets have two distinct shapes after pinching-off at junction J2. Depending on its size, the droplet can be spherical ($h > D_M$) or ellipsoidal ($h < D_M$), Figure 3b. Here, D_M is the measured outer diameter of the double-emulsion droplets, and h is the channel height. In the earlier case, the measured diameter of the droplet was the actual diameter. In the latter case, the equivalent diameter was calculated indirectly through the volume of the ellipsoid. The volume of an ellipsoid consists of a major and minor axis length $D_M/2$ and $h/2$ is

$$V_{Ellipsoid} = \frac{1}{6}\pi {D_M}^2 h \quad (5)$$

Balancing eq 5 with the volume of a sphere leads to equivalent diameter D_{Eq}:

$$\frac{1}{6}\pi {D_{Eq}}^3 = \frac{1}{6}\pi {D_M}^2 h$$

$$D_{Eq} = \sqrt[3]{{D_M}^2 h} \quad (6)$$

RESULTS AND DISCUSSION

Numerical Analysis and Experimental Validation on Microchannel Deformation under Device Stretching. We numerically investigated the deformation of the microchannel design with 50-μm constriction under various elongations. The numerical analysis was conducted using COMSOL Multiphysics version 5.4. Supporting Information S-5 provides details of the simulation. We found that stretching individual junctions would not affect other junctions, Figure 4. Stretching junction J1 increases the width of the core phase inlet (W_{CP}), the constriction (W_{C1}), and the core outlet (W_{CO}). In contrast, stretching J1 reduces the constriction length (L_{C1}), shell phase channel width (W_{SP}), and channel height (H), Figure 4a(i). According to the numerical results presented in Figure 4a(ii), stretching J1 did not affect the channel dimensions at J2, which was later validated by experiments. The results confirmed the effectiveness of our strategy of isolating individual junctions for stretching. Similarly, stretching junction J2 increases the width of the constriction (W_{C2}) and double-emulsion outlet channel (W_{DEO}). In contrast, stretching J2 reduces the constriction length (L_{C2}), carrier phase channel width (W_{CRP}), and channel height (H), Figure 4b(i). Also, stretching J2 did not affect the dimensions of J1, Figure 4b(ii). Finally, stretching the entire device shows the same variation of J1 and J2 as observed in the two cases mentioned above, as shown in Figure 4c(i),(ii).

Stretching Junction J1. This work used a two-step flow-focusing configuration to form the double emulsions. The effect of stretching on double-emulsion formation was conducted under three different cases: stretching junction 1, stretching junction 2, and stretching the entire device.

Stretching J1 caused the size of the core droplets to increase. Uniform core encapsulation was observed for elongation from 1 mm (81.08 ± 1.35 μm) to 3 mm (86.88 ± 1.72 μm), Figure 5a(i). However, core droplets at 4 mm elongation were polydispersed due to splitting at J2 because of the increasing core size (81.78 ± 23.34 μm). As the core size increases, the outer diameter of the shell phase also increases, Figure 5a. The shell thickness is consistent throughout elongations from 1 to 3 mm. However, a highly varying shell thickness can be observed at 4 mm elongation. We observed empty droplets and increasing size at J2, Figure 5a(ii). The shell phase that separates two core droplets in the fluid stream after J1 forms empty droplets. As J1 is stretched, the droplet spacing

https://doi.org/10.1021/acs.analchem.5c00338
Anal. Chem. XXXX, XXX, XXX−XXX

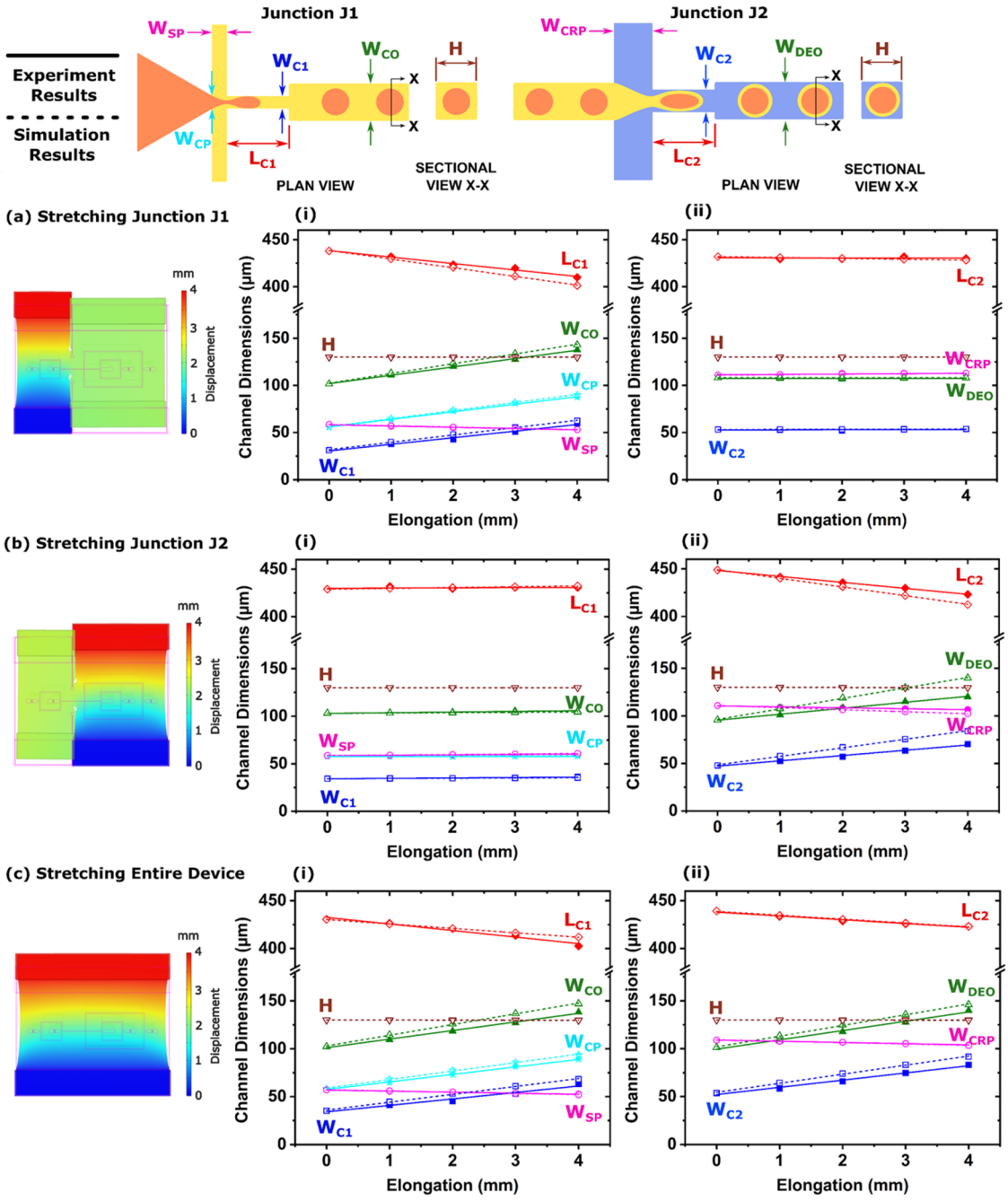

Figure 4. Experimental and numerical results of channel dimensions under the three stretching cases. (a) Change of critical channel dimensions at J1 and J2 with only stretching J1. (b) Change of critical channel dimensions at J1 and J2 with only stretching J2. (c) Change in critical channel dimensions at J1 and J2 with stretching the entire device. The initial dimensions of the first flow-focusing microchannel before stretching: width of the core phase inlet (W_{CP}) ~ 50 μm, constriction width (W_{C1}) ~ 30 μm, constriction length (L_{C1}) ~ 450 μm, width of core outlet channel (W_{CO}) ~ 100 μm, and the width of the shell phase channel (W_{SP}) ~ 40 μm. The initial dimensions of the second flow-focusing microchannel before stretching: constriction width (W_{C2}) ~ 50 μm, constriction length (L_{C2}) ~ 450 μm, width of double-emulsion outlet channel (W_{DEO}) ~ 100 μm, and width of carrier phase channel (W_{CRP}) ~ 100 μm. All of the microchannels have the same height (H) of ~130 μm.

increases, resulting in larger empty droplets at J2. The empty droplets were formed intermittently with double-emulsion droplets, see Video S4. Overall, stretching junction J1 showed an 84% core volume increase for the 80 μL/h total flow rate condition, Figure 5a, where the core phase flow rate is 20 μL/h and the shell phase flow rate is 60 μL/h.

Stretching Junction J2. Stretching J2 enlarges the outer diameter of the double-emulsion droplets and reduces the formation frequency. Monodisperse double emulsions were produced for all of the elongations. The core droplets showed a relatively consistent size across all elongations, Figure 5b. For the given flow rate conditions, the outer diameter of the double-emulsion droplets increased from 137.13 ± 2.64 to 143.72 ± 1.03 μm, with stretching J2 from 0 to 4 mm. Hence, the resulting shell thickness increased from 25.72 ± 1.31 to 28.45 ± 0.93 μm. However, the shell phase exhibits jetting downstream before being pinched off with increasing elongations. This happened because of the reduced shear

https://doi.org/10.1021/acs.analchem.5c00338
Anal. Chem. XXXX, XXX, XXX−XXX

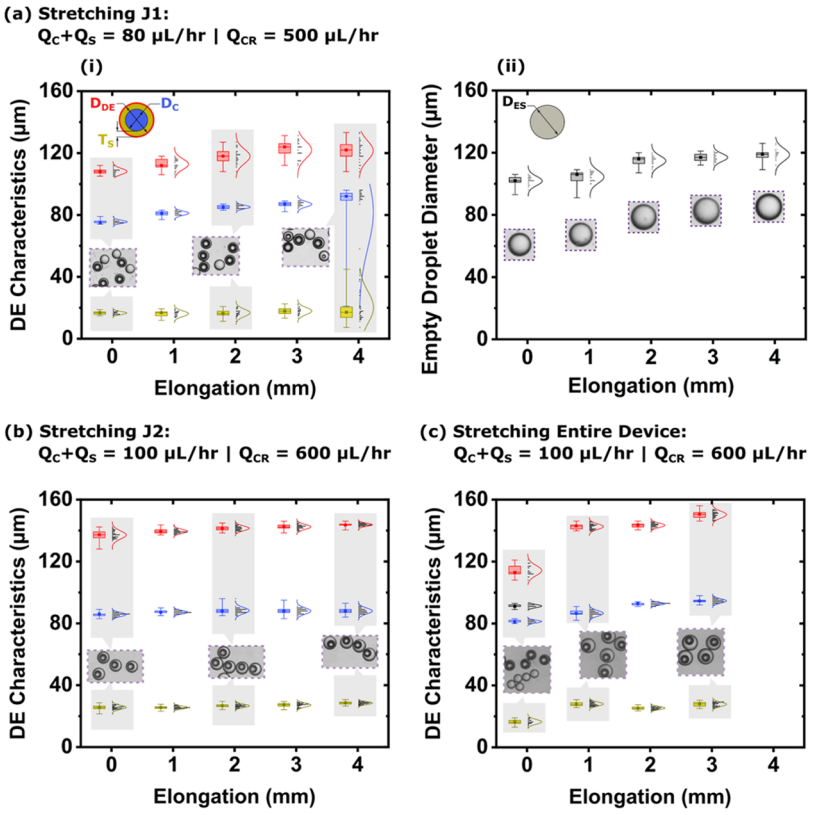

Figure 5. Experimental study of the effect of stretching (1−4 mm) on double-emulsion characteristics under the three stretching cases. (a) Stretching J1: (i) variation of core diameter (D_C) (blue), double-emulsion outer diameter (D_{DE}) (red), and shell thickness (T_S) (yellow) and (ii) empty shell droplet diameter (D_{ES}) (gray); (b) stretching J2: D_C (blue), D_{DE} (red), and T_S (yellow); (c) stretching entire device: D_C (blue), D_{DE} (red), T_S (yellow), and D_{ES} (gray).

force on the shell fluid with increasing constriction width, accumulating more shell fluid before pinching-off. In addition, partial wetting of the microchannel walls with the shell phase can be observed during jetting. However, more uniform droplets were observed at higher elongations, see Video S5. Overall, stretching junction J2 showed a 23% shell volume increase for the 80 μL/h total flow rate condition, where the core phase flow rate is 20 μL/h and the shell phase flow rate is 60 μL/h.

Stretching the Entire Device. Stretching the entire device (both J1 and J2 simultaneously) enlarged both the core and double-emulsion droplet, hence leading to a thicker shell. The core size increased with stretching, with good uniformity at the tested elongations, Figure 5c. Under zero elongation, early pinch-off resulted in a smaller outer diameter of the shell phase, intermittently forming empty shell droplets. However, if the device was stretched further, then the pinch-off dynamics became more consistent, showing an increasing outer diameter with increasing elongation. Hence, the shell was thicker compared to that under unstretched condition. Overall, 2 mm elongation produced monodispersed droplets with uniform core size (92.74 ± 0.92 μm) and shell thickness (25.35 ± 0.96 μm) for the 100-μL/h condition. However, 4 mm elongation did not produce stable double emulsion because of instability due to wetting of the channel wall with the shell phase, see Video S6.

The above subsections primarily discussed the effect of device elongation under selected fixed flow rate conditions, where monodisperse double emulsion can be generated. However, it is important to investigate the effect of flow conditions on the formation of double emulsion in a stretchable microfluidic device. So, we further analyzed the effect of altering the flow rates of the core, shell, and carrier fluid phases on double-emulsion characteristics. This discussion can be found in the Supporting Information S-6. From the results, we concluded that the effect of stretching has a significant influence on the characteristics of the double emulsion compared to the change in flow conditions within the experimented range. In addition, achieving monodisperse double emulsions in rigid devices is challenging, as generation frequencies of the core and the double emulsion have to match. However, the flexible devices show promising results, even with frequency mismatch.

Estimation of Scaling Law Parameters. We further estimated the values of parameters k_{ij}, m_{ij}, k'_{ij}, and m'_{ij} in eqs 1 and 2 based on experimental data of core size, core generation frequency, double-emulsion size, and double-emulsion generation frequency. Data fitting for the exponential function was conducted. Details can be found in Supporting Information S-7. Figure 6 depicts the fitted data for the case of stretching the entire device under 100-μL/h. Figure 6a,b shows the normalized sizes of the core and double emulsion. Figure 6c,d show the respective pinch-off times of core and double-emulsion droplets against the stretching variable α. The behavior shows a good fit in power laws, within 95% confidence bounds. That means, the double-emulsion characteristics increase with increasing elongation. The determined parameters for the generated cores (k_{31} = 1.377, m_{31} = 0.3002, k'_{31} = 0.5138, and m'_{31} = 0.5973) and generated double-emulsion droplets (k_{32} = 1.273, m_{32} = 0.2961, k'_{32} =

https://doi.org/10.1021/acs.analchem.5c00338
Anal. Chem. XXXX, XXX, XXX−XXX

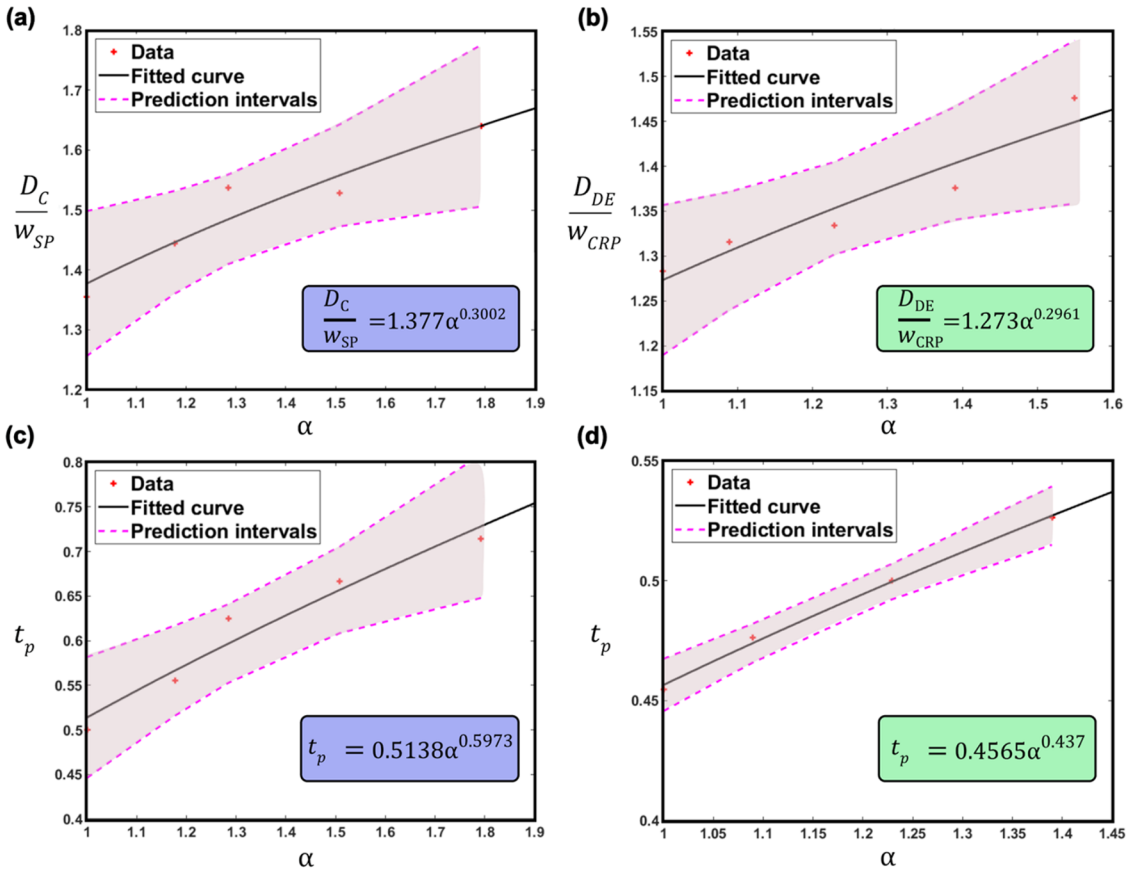

Figure 6. Experimental data and fitted correlations in power laws for case 3 (stretching the entire device) unde Q_C: 20 μL/h, Q_S: 60 μL/h, Q_{CRP}: 500 μL/h. (a) Normalized core size against stretching variable; (b) normalized outer diameter of the double-emulsion droplet against stretching variable; (c) core pinch-off time against stretching variable; (d) double-emulsion pinch-off time against stretching variable.

0.4565, and m'_{32} = 0.437) indicate that the sizes increase with increasing elongation, while showing a decrease in generation frequency. That means that the device geometry significantly affects the double-emulsion characteristics compared to changes in flow rate conditions. It should be noted that the evaluated parameters from curve fitting are specific to the device design and channel configuration and may differ for devices with other geometry.

Calhoun et al. comprehensively studied the effect of flow rates on double-emulsion droplet volume.[30] The team produced monodispersed single-core double-emulsion droplets with a core volume-to-shell volume ratio ranging from 0.181 to 0.703 by varying core (110−230 μL/h) and shell (280−760 μL/h) flow rates, while maintaining a constant flow rate for the carrier phase. However, our recent study[16] showed that the effect of device geometry significantly alters double-emulsion characteristics compared to changing flow rates of the fluid phases. Besides, changing microchannel dimensions to generate double emulsions of different sizes is cumbersome. Therefore, microfluidic devices that can change dimensions by stretching will address this problem. The dimensional tunability of flexible devices avoids the repetitive design of microfluidic devices with different dimensions. Therefore, micro-elastofluidic technology for double-emulsion formation would be more cost-effective and time-efficient than conventional rigid-device technology.

CONCLUSIONS

This paper reports a fully flexible, stretchable microfluidic device for generating tunable double emulsion. The double emulsion was formed in a two-step flow-focusing microchannel design. The variation of microchannel dimensions, such as width and height, was evaluated numerically and experimentally. The agreement between the numerical and experimental results confirms our method of isolating and stretching the junctions individually. Theoretical analysis and experiments were conducted to decipher the influence of stretching on double-emulsion generation. In general, laterally stretching increases the core size and shell thickness while reducing the generation frequency. Specifically, stretching the second flow-focusing junction J2, where the double-emulsions are formed, produces highly monodispersed double-emulsion droplets with increasing shell thickness. The results demonstrated an increase of ∼84% in the core volume and an increase of ∼23% in the shell volume for a device strain of only ∼16%. We believe that this innovative, flexible droplet microfluidic platform will provide an alternative way to precisely control the double-emulsion formation dynamics by modifying the channel dimensions on site and in real-time without redesigning and refabricating the devices.

ASSOCIATED CONTENT

Supporting Information

The Supporting Information is available free of charge at https://pubs.acs.org/doi/10.1021/acs.analchem.5c00338.

https://doi.org/10.1021/acs.analchem.5c00338
Anal. Chem. XXXX, XXX, XXX−XXX

Fundamentals of double-emulsion generation under the effect of device elongation; physical properties of fluids used for the experiments; dynamics of double-emulsion formation in the fabricated two-step microfluidic devices; experimental study on the effect of flow rates and device geometry on monodisperse double-emulsion formation; numerical modeling of microfluidic device stretching; the effects of flow conditions on double-emulsion formation; estimated scaling law parameters. (DOCX)

Video S1: Video recorded during the experiment conducted for double-emulsion formation in a flexible microfluidic device (Figure 3). (MP4)

Video S2: Video recorded during the experiment conducted for evaluating double-emulsion formation dynamics (Figure S2). (MP4)

Video S3.1: Video recorded during the experiment conducted for evaluating double-emulsion formation dynamics (Figure S2a). (MP4)

Video S3.2: Video recorded during the experiment conducted for evaluating the effect of flow rate and device geometry on monodisperse double-emulsion formation (Figure S3b). (MP4)

Video S4: Video recorded during the experiment reported in case 1 (Figure 5a). (MP4)

Video S5: Video recorded during the experiment reported in case 2 (Figure 5b). (MP4)

Video S6: Video recorded during the experiment reported in case 3 (Figure 5c). (MP4)

AUTHOR INFORMATION

Corresponding Authors

Jun Zhang − *Queensland Micro and Nanotechnology Centre, Griffith University, Nathan, QLD 4111, Australia; School of Engineering and Built Environment, Griffith University, Nathan, QLD 4111, Australia;* orcid.org/0000-0003-1113-6264; Email: jun.zhang@griffith.edu.au

Nam-Trung Nguyen − *Queensland Micro and Nanotechnology Centre, Griffith University, Nathan, QLD 4111, Australia;* orcid.org/0000-0003-3626-5361; Email: nam-trung.nguyen@griffith.edu.au

Authors

Uditha Roshan − *Queensland Micro and Nanotechnology Centre, Griffith University, Nathan, QLD 4111, Australia;* orcid.org/0000-0002-8543-1373

Ajeet Singh Yadav − *Queensland Micro and Nanotechnology Centre, Griffith University, Nathan, QLD 4111, Australia*

Xiaoyue Kang − *Queensland Micro and Nanotechnology Centre, Griffith University, Nathan, QLD 4111, Australia*

Du Tuan Tran − *Queensland Micro and Nanotechnology Centre, Griffith University, Nathan, QLD 4111, Australia*

Amith Mudugamuwa − *Queensland Micro and Nanotechnology Centre, Griffith University, Nathan, QLD 4111, Australia*

Complete contact information is available at: https://pubs.acs.org/10.1021/acs.analchem.5c00338

Author Contributions

N.-T.N. and J.Z.: conceptualization, supervision, and project administration. U.R.: formal analysis, numerical simulations, device fabrication, experiments, writing−original draft, and visualization. A.S.Y., X.K., D.T.T., and A.M.: experiments. J.Z. and N.-T.N.: writing−review and editing. N.-T.N. and J.Z.: funding acquisition. All of the authors provided critical feedback and read and approved the manuscript.

Notes

The authors declare no competing financial interest.

ACKNOWLEDGMENTS

U.R. acknowledges the support of the higher degree research scholarship from Griffith University. This work was partly performed at the Queensland node of the Australian National Fabrication Facility (ANFF). A company established under the National Collaborative Research Infrastructure Strategy (NCRIS) to provide nano and microfabrication facilities for Australia's researchers. Also, the authors acknowledge the support from the Australian Research Council (ARC) Australian Laureate Fellowship (Grant No. FL230100023) and ARC Future Fellowship (Grant No. FT240100020).

REFERENCES

(1) Utada, A. S.; Lorenceau, E.; Link, D. R.; Kaplan, P. D.; Stone, H. A.; Weitz, D. *Science* **2005**, *308* (5721), 537−541.

(2) Galogahi, F. M.; Ansari, A.; Teo, A. J.; Cha, H.; An, H.; Nguyen, N.-T. *Biomed. Microdevices* **2022**, *24* (4), 40.

(3) Chan, H. F.; Zhang, Y.; Ho, Y.-P.; Chiu, Y.-L.; Jung, Y.; Leong, K. W. *Sci. Rep.* **2013**, *3* (1), No. 3462.

(4) Nie, H.; Fu, Y.; Wang, C.-H. *Biomaterials* **2010**, *31* (33), 8732−8740.

(5) Augustin, M. A.; Hemar, Y. *Chem. Soc. Rev.* **2009**, *38* (4), 902−912.

(6) Peña, B.; Panisello, C.; Aresté, G.; Garcia-Valls, R.; Gumí, T. *Chem. Eng. J.* **2012**, *179*, 394−403.

(7) Tran, D. T.; Nguyen, N. K.; Yadav, A. S.; Chuang, A.; Burford, M.; Galogahi, F. M.; Sreejith, K. R.; Nguyen, N. T. *Adv. Energy Sustainability Res.* **2024**, *5* (7), No. 2400112.

(8) Galogahi, F. M.; Christie, M.; Yadav, A. S.; An, H.; Stratton, H.; Nguyen, N.-T. *Analyst* **2023**, *148* (17), 4064−4071.

(9) Galogahi, F. M.; Strachan, S.; Yadav, A. S.; Stratton, H.; Nguyen, N. T. *Adv. NanoBiomed Res.* **2024**, *4* (12), No. 2400044.

(10) Ding, S.; Serra, C. A.; Vandamme, T. F.; Yu, W.; Anton, N. *J. Controlled Release* **2019**, *295*, 31−49.

(11) Galogahi, F. M.; Zhu, Y.; An, H.; Nguyen, N.-T. *J. Sci.: Adv. Mater. Devices* **2020**, *5* (4), 417−435.

(12) Vashi, A.; Yadav, A. S.; Nguyen, N.-T. *Colloids Surf., A* **2024**, *702*, No. 135185.

(13) Yadav, A. S.; Tran, D. T.; Teo, A. J.; Dai, Y.; Galogahi, F. M.; Ooi, C. H.; Nguyen, N.-T. *Micromachines* **2023**, *14* (3), 497.

(14) Okushima, S.; Nisisako, T.; Torii, T.; Higuchi, T. *Langmuir* **2004**, *20* (23), 9905−9908.

(15) Nie, Z.; Seo, M.; Xu, S.; Lewis, P. C.; Mok, M.; Kumacheva, E.; Whitesides, G. M.; Garstecki, P.; Stone, H. A. *Microfluid. Nanofluid.* **2008**, *5*, 585−594.

(16) Galogahi, F. M.; Zhu, Y.; An, H.; Nguyen, N.-T. *Microfluid. Nanofluid.* **2021**, *25*, 82.

(17) Liu, H.; Zhang, Y. *Phys. Fluids* **2011**, *23* (8), No. 082101.

(18) McClements, D. J.; Decker, E. A. *J. Food Sci.* **2000**, *65* (8), 1270−1282.

(19) Heidari, F.; Jafari, S. M.; Ziaiifar, A. M.; Malekjani, N. *Adv. Colloid Interface Sci.* **2022**, *299*, No. 102567.

(20) Yadav, A. S.; Galogahi, F. M.; Vashi, A.; Tran, D. T.; Kijanka, G. S.; Cha, H.; Sreejith, K. R.; Nguyen, N.-T. *Biomed. Microdevices* **2024**, *26* (2), 24.

(21) Teo, A. J. T.; Malekpour-galogahi, F.; Sreejith, K. R.; Takei, T.; Nguyen, N.-T. *AIP Adv.* **2020**, *10* (6), No. 065101.

(22) Roshan, U.; Mudugamuwa, A.; Cha, H.; Hettiarachchi, S.; Zhang, J.; Nguyen, N.-T. *Lab Chip* **2024**, *24* (8), 2146−2175.

(23) Roshan, U.; Dai, Y.; Yadav, A. S.; Hettiarachchi, S.; Mudugamuwa, A.; Zhang, J.; Nguyen, N.-T. *Sens. Actuators, B* **2025**, *422*, No. 136617.
(24) Kim, P.; Kwon, K. W.; Park, M. C.; Lee, S. H.; Kim, S. M.; Suh, K. Y. *Biochip J.* **2008**, *2*, 1−11.
(25) Fallahi, H.; Zhang, J.; Nicholls, J.; Phan, H.-P.; Nguyen, N.-T. *Anal. Chem.* **2020**, *92* (18), 12473−12480.
(26) Trantidou, T.; Elani, Y.; Parsons, E.; Ces, O. *Microsyst. Nanoeng.* **2017**, *3* (1), 16091.
(27) Lashkaripour, A.; McIntyre, D. P.; Calhoun, S. G.; Krauth, K.; Densmore, D. M.; Fordyce, P. M. *Nat. Commun.* **2024**, *15* (1), No. 83.
(28) Matsumoto, K.; Sogabe, S.; Endo, T. *J. Polym. Sci., Part A: Polym. Chem.* **2010**, *48* (20), 4515−4521.
(29) Basu, A. S. *Lab Chip* **2013**, *13* (10), 1892−1901.
(30) Calhoun, S. G. K.; Brower, K. K.; Suja, V. C.; Kim, G.; Wang, N.; McCully, A. L.; Kusumaatmaja, H.; Fuller, G. G.; Fordyce, P. M. *Lab Chip* **2022**, *22* (12), 2315−2330.

https://doi.org/10.1021/acs.analchem.5c00338
Anal. Chem. XXXX, XXX, XXX−XXX